

This is a self-archived version of an original article. This version may differ from the original in pagination and typographic details.

Author(s): Ikonen, Joni; Möttönen, Mikko

Title: Accelerated stabilization of coherent photon states

Year: 2018

Version: Published version

Copyright: © 2018 The Author(s)

Rights: CC BY 3.0

Rights url: <http://creativecommons.org/licenses/by/3.0/>

Please cite the original version:

Ikonen, J., & Möttönen, M. (2018). Accelerated stabilization of coherent photon states. *New Journal of Physics*, 20(October), Article 103047. <https://doi.org/10.1088/1367-2630/aae621>

PAPER • OPEN ACCESS

Accelerated stabilization of coherent photon states

To cite this article: Joni Ikonen and Mikko Möttönen 2018 *New J. Phys.* **20** 103047

View the [article online](#) for updates and enhancements.



IOP | ebooks™

Bringing you innovative digital publishing with leading voices to create your essential collection of books in STEM research.

Start exploring the collection - download the first chapter of every title for free.



PAPER

Accelerated stabilization of coherent photon states

Joni Ikonen¹ and Mikko Möttönen^{1,2}¹ QCD Labs, QTF Centre of Excellence, Department of Applied Physics, Aalto University, FI-00076 Aalto, Finland² University of Jyväskylä, Department of Mathematical Information Technology, PO Box 35, FI-40014 University of Jyväskylä, FinlandE-mail: joni.2.ikonen@aalto.fi**Keywords:** quantum control, circuit quantum electrodynamics, dissipative quantum systems, quantum state preparation, tunable electromagnetic environments

RECEIVED

26 June 2018

REVISED

10 September 2018

ACCEPTED FOR PUBLICATION

4 October 2018

PUBLISHED

31 October 2018

Original content from this work may be used under the terms of the [Creative Commons Attribution 3.0 licence](#).

Any further distribution of this work must maintain attribution to the author(s) and the title of the work, journal citation and DOI.



Abstract

Control and utilization of coherent states of microwave photons is a ubiquitous requirement for the present and near-future implementations of solid-state quantum computers. The rate at which the photon state responds to external driving is limited by the relaxation rate of the storage resonator, which poses a trade-off between fast control and long storage time. Here, we present a control scheme that is designed to drive an unknown photon state to a desired coherent state much faster than the resonator decay rate. Our method utilizes a tunable environment which acts on an ancillary qubit coupled to the resonator. By periodically resetting the qubit and tuning it into resonance with the resonator, possible photon loss and dephasing of the resonator mode are corrected without measurements or active feedback. In general, our method is suitable for accelerating the control of coherent states in high-fidelity resonators.

1. Introduction

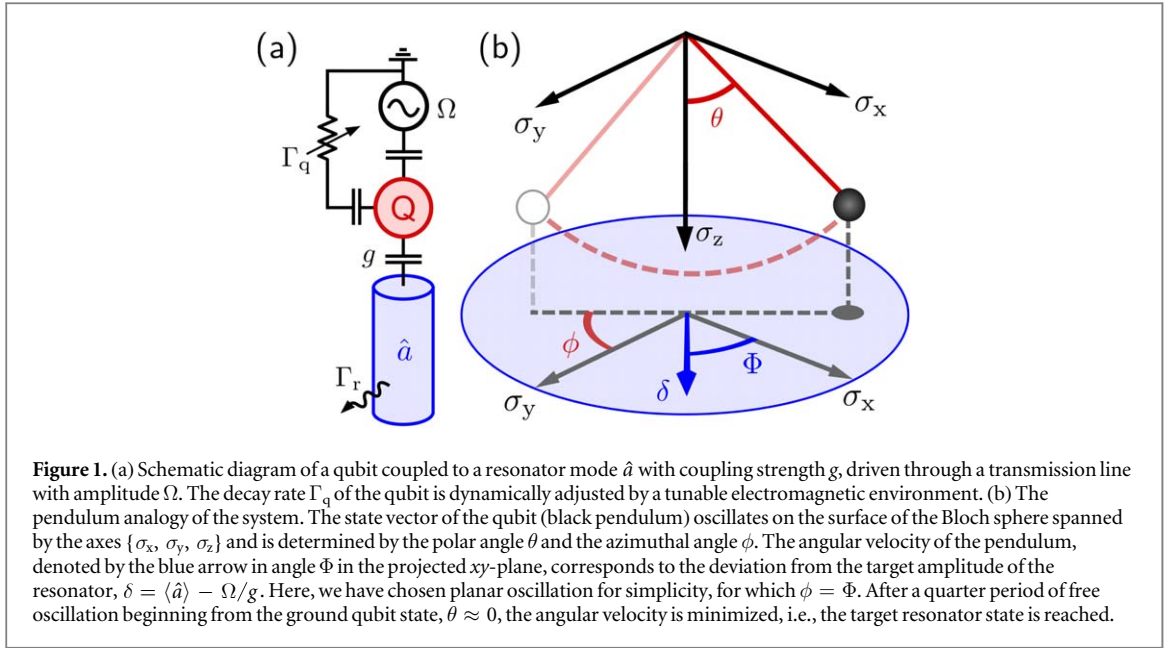
The storage and manipulation of the quantum state of photons is an integral part of the implementation of quantum information processing [1–3] in the field of quantum electrodynamics [4]. In particular, coherent states of photons serve as the starting point or a reference state in various applications including dispersive readout of qubits [5], state tomography of itinerant photon fields [6], and encoding of quantum information [7–9].

Coherent states are typically inserted and maintained in a superconducting resonator or cavity by coherently driving the device until the out-going photon flux equals the intensity of the in-coming signal. However, this involves a trade-off between long lifetime of the stored state after driving and fast response to control, because both of these properties are tied to the quality factor of the device. Some speed up may be obtained by temporarily increasing the drive power, but this is advantageous only if the initial state is accurately known. Several methods to tackle this trade-off have been demonstrated recently. These include the adjustment of the external quality factor of the storage resonator using a tunable coupler [10, 11] or a flux-driven Josephson junction [12], and conversion from stationary to propagating photons using a driven transmon qubit [13] or a Josephson ring modulator [14].

There have also been recent efforts [15, 16] to rapidly reset the resonator mode to the vacuum state which coincides with a coherent state of zero amplitude. The combination of coherent driving and dissipation has been utilized to stabilize also non-classical cat states [17, 18].

In this work, we tackle the trade-off problem by utilizing tunable electromagnetic environments such as the recently demonstrated quantum-circuit refrigerator [19, 20] (QCR). Coupled to a quantum device such as a resonator or a qubit, the QCR allows fast and flexible control over the relaxation rate of the coupled element. Consequently, it may be used to reset a qubit to the ground state in a time scale much shorter than the natural lifetime.

In our stabilization protocol, we maintain the state of a slowly dissipating resonator mode without active monitoring. The stabilizing effect arises from resonant interactions with a qubit that is driven at a constant amplitude and is periodically reset to the ground state by, for example, a QCR. As a result, the resonator state



converges towards a chosen coherent state at a rate that is proportional to the increased relaxation rate of the qubit. This rate can be tuned to be several orders of magnitude higher than the natural decay rate of a high-quality resonator and is primarily limited by the qubit–resonator coupling strength. Notably, any losses, excitations, or phase shifts that occur in the resonator are corrected significantly faster than a simple continuous drive allows.

Our method serves to speed up the preparation and manipulation of resonator states which are the most time-consuming tasks of many quantum information protocols. It is particularly well suited to mitigate errors from slow decay and dephasing of the resonator state. In addition, the stabilization protocol can be used to reduce the amount of thermal photons in a resonator by transferring them to the qubit and subsequently to the tunable environment. In contrast to the recently demonstrated reset schemes [15, 16], our approach does not require any prior information about the state of the system. This allows resonator initialization in systems where directly coupling the storage resonator to a cold bath is not desirable. Interestingly, our approach evacuates the thermal photons also while stabilizing to a finite-amplitude coherent state, a feature which may render a separate cooling phase unnecessary in resonator state control.

Moreover, our stabilization method presents a complementary application for the tunable response rate of a resonator. Whereas recent experiments that have realized effectively tunable quality factors are motivated by fast injection of arbitrary photon states to the resonator [11–13], we envisage protocols where ancillary coherent states are repeatedly stabilized and reused for various tasks. On the other hand, in previous work [21] we have shown that maintaining a coherent state in this manner may be beneficial in reducing harmful heat loads subject to quantum circuits. To this end, the present work potentially offers a faster and more conveniently realizable approach.

This work is organized in the following way. In section 2, we describe our physical system and derive an approximate model from the full Hamiltonian. In section 3, we introduce the stabilization sequence and use both numerical simulations and the simplified model to calculate the effective stabilization rate, i.e., the rate at which the mode converges towards the target state. We also apply our method to the problem of resetting a resonator to the vacuum state, evacuating initial photons at a rate that is independent of the decay rate of the bare resonator. The stabilization results are summarized and discussed in section 4.

2. Theory

We consider a system consisting of a tunable qubit coupled to a transmission line and a single mode of a microwave resonator, as depicted in figure 1(a). We treat the mode as a harmonic oscillator with angular frequency ω , and the qubit as a two-level system with transition frequency $\omega_q(t) = \omega + \Delta(t)$, where $\Delta(t)$ is the controllable detuning. The qubit is driven through the transmission line at angular frequency ω with complex amplitude Ω . In addition, the qubit can be exposed on demand to the strongly dissipative environment of a QCR. We do not analyze the dynamics of the QCR in this work explicitly, but instead assume that the relaxation rate of the qubit is a dynamically controllable variable $\Gamma_q(t)$.

2.1. Displaced reference frame due to a driven qubit

Before investigating this setup in full detail in section 3, we analyze the unitary evolution of our system without detuning and damping. In the frame rotating with angular frequency ω , where we make the rotating-wave approximation, the system is described by the Jaynes–Cummings Hamiltonian

$$\hat{H} = \hbar g (\hat{a} \otimes \hat{\sigma}_+ + \hat{a}^\dagger \otimes \hat{\sigma}_-) + \hbar \hat{I} \otimes (\Omega \hat{\sigma}_+ + \Omega^* \hat{\sigma}_-), \quad (1)$$

where g denotes the coupling strength between the mode and the qubit, \hat{I} is the identity operator, and \hat{a} and $\hat{\sigma}_- = |g\rangle\langle e|$ are the annihilation operators of the mode and the qubit, respectively. Here, $|g\rangle$ and $|e\rangle$ denote the ground and excited state of the qubit, respectively.

By re-grouping the terms as

$$\hat{H} = \hbar g \left(\hat{a} + \frac{\Omega}{g} \hat{I} \right) \otimes \hat{\sigma}_+ + \hbar g \left(\hat{a}^\dagger + \frac{\Omega^*}{g} \hat{I} \right) \otimes \hat{\sigma}_-, \quad (2)$$

and noting that the unitary displacement operator $\hat{D}(x) = \exp(x\hat{a}^\dagger - x^*\hat{a})$ acts on \hat{a} as $\hat{D}(x)\hat{a}\hat{D}^\dagger(x) = \hat{a} - x\hat{I}$, we may interpret \hat{H} as the Jaynes–Cummings interaction term in a frame displaced by $\alpha_T \equiv -\Omega/g$. Thus driving the qubit at the resonance frequency ω effectively shifts the origin of the resonator phase space to point α_T in the non-displaced frame. A useful consequence is that a coherent state $|\alpha_T + \delta\rangle \otimes |g\rangle$, where δ is an arbitrary complex number, naturally evolves towards another state $|\alpha_T\rangle \otimes |\psi\rangle$, where $|\psi\rangle \neq |g\rangle$. This is intuitively understood in the displaced frame, where the state $|\delta\rangle \otimes |g\rangle$ evolves towards the vacuum $|0\rangle \otimes |\psi\rangle$ as the mode exchanges an excitation with the qubit. This is the core mechanism of the stabilization method introduced in section 3.

2.2. Approximation assuming separable states

To describe the above-mentioned dynamics analytically, we approximate the system as two separable components, such that the states of the components are represented by vectors of the respective uncoupled Hilbert spaces. Furthermore, we assume that the mode is fully described by a coherent state, the amplitude of which deviates from α_T by a complex number $\delta(t) = |\delta(t)| e^{i\phi(t)}$, that is, $\hat{a}|\alpha_T + \delta(t)\rangle = [\alpha_T + \delta(t)]|\alpha_T + \delta(t)\rangle$. We parametrize the qubit state vector as

$$|q(t)\rangle = \cos[\theta(t)/2]|g\rangle - ie^{i\phi(t)}\sin[\theta(t)/2]|e\rangle, \quad (3)$$

where θ and ϕ denote the polar and azimuthal angles of the Bloch vector, as shown in figure 1(b). Thus the degrees of freedom in the system are reduced to the complex deviation $\delta(t)$ and the two real angles $\theta(t)$ and $\phi(t)$.

The resonator mode and the qubit are separately controlled by the effective Hamiltonians

$$\begin{aligned} \hat{H}_r(t) &= \langle q(t) | \hat{H} | q(t) \rangle = \frac{i}{2} \hbar g \sin[\theta(t)] \\ &\times [e^{-i\phi(t)}(\hat{a} - \alpha_T) - e^{i\phi(t)}(\hat{a}^\dagger - \alpha_T^*)], \end{aligned} \quad (4)$$

$$\begin{aligned} \hat{H}_q(t) &= \langle \alpha_T + \delta(t) | \hat{H} | \alpha_T + \delta(t) \rangle \\ &= \hbar g \delta(t) \hat{\sigma}_+ + \hbar g \delta^*(t) \hat{\sigma}_-, \end{aligned} \quad (5)$$

respectively. We note that \hat{H}_q describes driving the qubit with an effective complex amplitude $g\delta(t)$ which rotates the Bloch vector at an angular frequency $2g|\delta(t)|$ about an axis that lies on the xy -plane with the azimuthal angle $\Phi(t)$. Furthermore, the Hamiltonian \hat{H}_r is a driving term that displaces the center of the coherent distribution at a rate

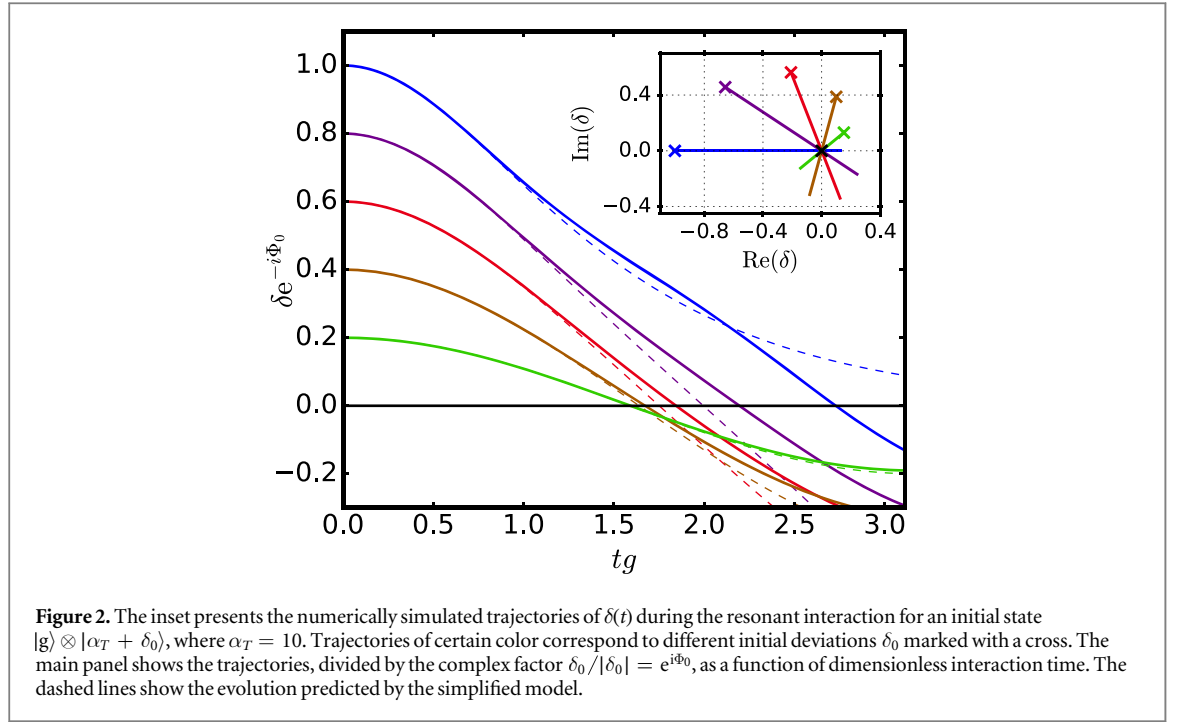
$$\dot{\delta}(t) = -\frac{1}{2}g \sin[\theta(t)]e^{i\phi(t)}. \quad (6)$$

For our purposes, it is sufficient to restrict our following solution to initial condition $\phi(0) = \Phi(0)$, i.e., $\hat{H}_q(0)$ will rotate the Bloch vector about an axis that is perpendicular to its initial great circle. Consequently, the phases of both the qubit and the deviation will remain constant, $\phi(t) = \Phi(t) = \Phi(0)$. Using equation (6) with $\dot{\theta}(t) = 2g|\delta(t)|$ and choosing the correct sign yields

$$\ddot{\theta}(t) = -g^2 \sin \theta(t), \quad (7)$$

which is the equation of a simple pendulum. The closed-form solution for the relevant initial conditions is presented in appendix A.

For $|\delta_0| = |\delta(0)| < 1$, the system will oscillate about the equilibrium state $\delta = \theta = 0$ in a way similar to a simple pendulum that does not have enough momentum to tip over the apex, see figure 1(b). The sign of $\theta_0 = \theta(0)$ determines whether the oscillation is advanced or delayed compared with the case where $\theta_0 = 0$. In terms of this analogy, the stabilization method is designed to let the system freely oscillate close to the turning



point where $\dot{\theta} \propto \delta \approx 0$, and then reset the qubit to $\theta = 0$. Repeating the process eventually drives the system to the equilibrium state.

2.3. Numerical verification of the simplified model

We numerically simulate the full dynamics of the Hamiltonian in equation (1) and compare the results to our simplified model. Figure 2 shows the temporal evolution of the amplitude deviation for an initial coherent state $|\alpha_T + \delta_0\rangle$, evaluated as $\delta(t) = \langle \hat{a} \otimes \hat{I} \rangle(t) - \alpha_T$. We observe that the simplified model accurately describes the dynamics for small δ_0 . For δ_0 close to unity, the differences are largely explained by the increased entanglement between the two subsystems which is ignored in the simplified model. Note that according to the simplified model, the magnitude of α_T has no effect on the dynamics, and poses only negligible differences in the numerical solution. The interaction times in our stabilization method below are limited to the quarter period interval $tg \leq \pi/2$.

3. State stabilization method

3.1. Master equation for the full stabilization sequence

We detune the qubit in and out of resonance to control the duration of the resonant interaction discussed above. This is represented by the addition of a term $\frac{1}{2}\Delta(t)\hat{\sigma}_z$ to the Hamiltonian in equation (1), where $\Delta(t) = \omega_q(t) - \omega$ is the time-controllable frequency detuning of the qubit. Additionally, the decay rate $\Gamma_q(t)$ of the qubit can be dynamically increased up to $\Gamma_{q,\max}$ using a QCR but is bound from below to reflect the finite natural lifetime of the qubit. With experimentally realistic parameters, the decay rate provided by the QCR ranges from $\Gamma_{q,\min} = 10^3 \frac{1}{s}$ to $\Gamma_{q,\max} = 5 \times 10^8 \frac{1}{s}$. We also assume a constant decay rate Γ_r of the resonator mode. The latter two assumptions are not necessary for the stabilization sequence but are included to simulate the method in a more realistic setting. The cross-coupling of the resonator mode to the QCR and the qubit drive line are assumed negligible. By neglecting the corrections on the dissipation arising from the effect of the drive and the qubit–resonator coupling, the total temporal evolution of the density operator $\hat{\rho}(t)$ of the system is given by the master equation

$$\begin{aligned} \dot{\hat{\rho}}(t) = & \frac{1}{i\hbar} \left[\hat{H} + \frac{\Delta(t)}{2} \hat{I} \otimes \hat{\sigma}_z, \hat{\rho}(t) \right] \\ & + \Gamma_q(t) \mathcal{L}[\hat{I} \otimes \hat{\sigma}_-] \hat{\rho}(t) + \Gamma_r \mathcal{L}[\hat{a} \otimes \hat{I}] \hat{\rho}(t), \end{aligned} \quad (8)$$

where $\mathcal{L}[\hat{A}] \hat{\rho} = \hat{A} \hat{\rho} \hat{A}^\dagger - \frac{1}{2} \hat{A}^\dagger \hat{A} \hat{\rho} - \frac{1}{2} \hat{\rho} \hat{A}^\dagger \hat{A}$ is the Lindblad superoperator. In the following sections, we solve this system numerically in a truncated Hilbert space [22].

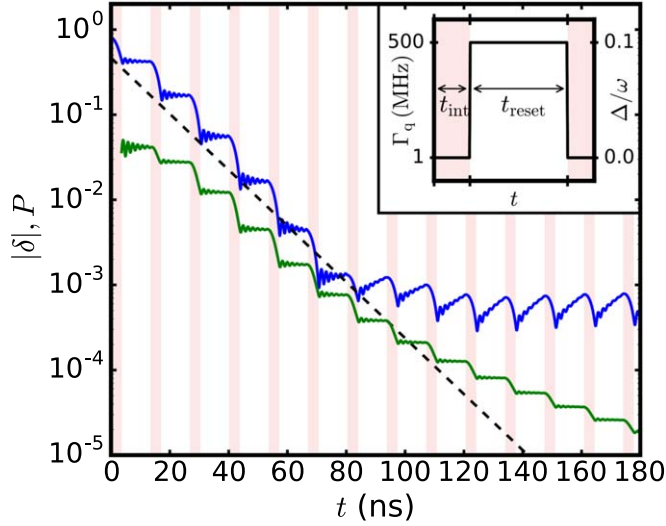


Figure 3. Amplitude deviation $\delta(t)$ from the target state (blue curve) and the lack of overlap $P(t)$ with the coherent state $|\alpha_T + \delta(t)\rangle$ (green curve), during a numerical simulation of the stabilization sequence applied to an initial state $|\alpha_T - 0.8\rangle \otimes |g\rangle$ with $\alpha_T = \sqrt{10}$. The sequence consists of alternating interaction and reset phases, indicated by pink and white backgrounds, respectively, during which the decay rate and the detuning of the qubit are varied as shown in the inset. The dashed line shows an exponential fit corresponding to an effective stabilization rate $\Gamma_{\text{eff}} \approx 76$ MHz. The parameters used in the simulation are $\omega/2\pi = 6$ GHz, $g/2\pi = 50$ MHz, $t_{\text{reset}} = 9.8$ ns, $t_{\text{int}} = 3.6$ ns and $\Gamma_r = 30$ kHz.

3.2. Stabilization

The purpose of the stabilization sequence is to drive the mode towards a chosen coherent state $|\alpha_T\rangle$ without active feedback. A single cycle of the sequence consists of an interaction phase and a reset phase, where $\Delta(t)$ and $\Gamma_q(t)$ assume values as illustrated in the inset of figure 3. Throughout the sequence, the qubit is driven with a constant amplitude $\Omega = -g\alpha_T$ at the resonator angular frequency ω . During the interaction phase, $\Delta(t) = 0$ and according to the results in section 2, a possible deviation δ in the resonator amplitude is expected to approach zero. In the reset phase, the qubit is detuned to off-resonance and exposed to strong damping which allows a controlled reset of the qubit towards the ground state while the resonator mode is ideally unaffected. The duration of the two phases, t_{int} and t_{reset} are required to be long enough to significantly reduce the deviation δ and to faithfully reset the qubit to the ground state. To this end, t_{int} and t_{reset} are chosen in section 3.3 to maximize the effective rate at which the deviation approaches zero.

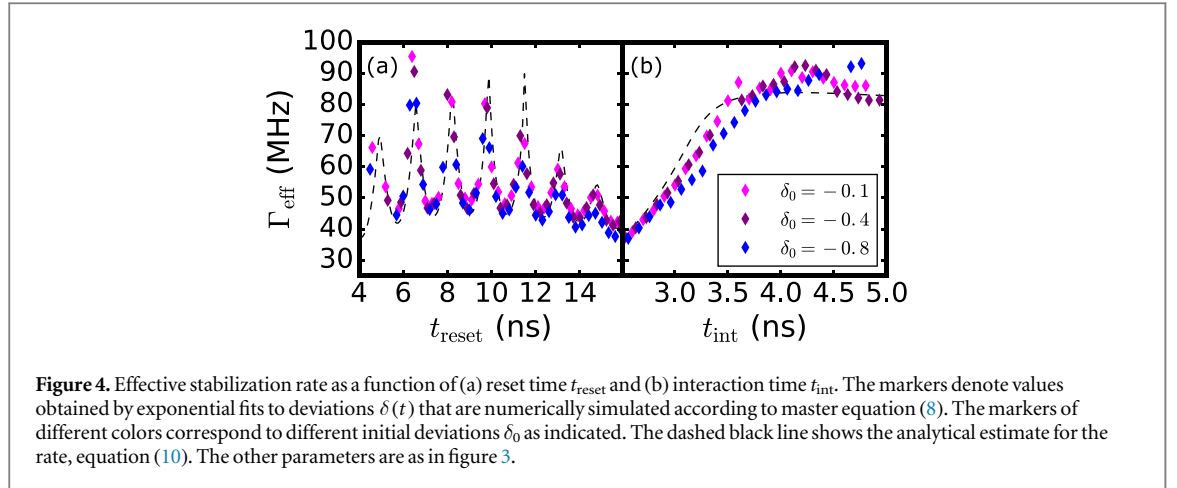
An example simulation of the full stabilization sequence is shown in figure 3. We observe that the deviation, evaluated by calculating the trace $\delta(t) = \text{Tr}[\hat{\rho}(t)\hat{a} \otimes \hat{I}] - \alpha_T$, faithfully decreases during the interaction phases and halts during resets. Importantly, the mode converges to the target state at a rate three orders of magnitude higher than the natural decay rate of the resonator. We also study the overlap between the system density operator and the coherent state of concurrent expectation value, namely $P(t) = 1 - \langle \alpha_T + \delta(t) | \text{Tr}_q[\hat{\rho}(t)] | \alpha_T + \delta(t) \rangle$, where Tr_q denotes a partial trace over the qubit degrees of freedom. The fast decrease of $P(t)$ confirms that the state indeed converges to the coherent state $|\alpha_T\rangle$ instead of any other state that satisfies $\langle \hat{a} \rangle = \alpha_T$.

As discussed above, the temporal evolution in the interaction phase and hence the rate of convergence are independent of α_T . Eventually, $\delta(t)$ reaches a plateau where the improvement gained during an interaction phase is lost owing to the constant decay of the mode during the following reset phase. Consequently, the deviation eventually oscillates between $|\delta_{\text{min}}| \approx \frac{1}{2}|\alpha_T| \Gamma_r t_{\text{int}}$ and $|\delta_{\text{max}}| \approx \frac{1}{2}|\alpha_T| \Gamma_r t_{\text{cycle}}$, where $t_{\text{cycle}} = t_{\text{int}} + t_{\text{reset}}$. Interestingly however, the overlap increases even when δ has reached the plateau.

Note that the above-made assumption of negligible crosstalk between the transmission line and the resonator is reasonable. We estimate this by adding to the above simulation a constant resonator drive term. The error caused by this leakage becomes comparable to the saturated error δ_{max} if the additional drive term is greater than $10^{-4} \times \Omega$. In addition to isolating the qubit drive from the resonator, we may nullify the effect of the crosstalk by a compensation tone. Namely, we drive the resonator exactly at the frequency of the qubit drive and choose the drive amplitude and phase such that it exactly cancels the crosstalk.

3.3. Effective stabilization rate

We define our figure of merit, the effective stabilization rate Γ_{eff} , as the rate at which the deviation exponentially approaches zero,



$$|\delta(t)| = |\delta_0| e^{-\Gamma_{\text{eff}} t}. \quad (9)$$

We derive an analytical estimate for the effective rate from the simplified model under the following assumptions. In the interaction phase, the system evolves according to equations (6) and (7). During a reset phase, the qubit decays at an increased rate $\Gamma_{q,\text{max}}$ and acquires a phase shift relative to the resonant oscillation due to the increased detuning. Allowing for the typical dispersive shift of the resonator mode frequency, the total phase shift between the mode and the qubit is proportional to $(\Delta + 2\frac{g^2}{\Delta})t_{\text{reset}}$. In appendix B, we show that the stabilization rate in the limit of small deviations $\delta, \theta \ll 1$ and infinite number of cycles is given by

$$\Gamma_{\text{eff}} = \frac{\Gamma_{q,\text{max}}}{4} \frac{t_{\text{reset}}}{t_{\text{cycle}}} - \frac{1}{t_{\text{cycle}}} \ln |\mu \pm \sqrt{\mu^2 - 1}|, \quad (10)$$

for $\text{Re}(\mu) \gtrless 0$, where

$$\mu = \cosh \left[\left(\frac{\Gamma_{q,\text{max}}}{4} - i\frac{\Delta}{2} - i\frac{g^2}{\Delta} \right) t_{\text{reset}} \right] \cos(gt_{\text{int}}). \quad (11)$$

This shows that the rate of stabilization is essentially proportional to the tunable decay rate of the qubit. This is in contrast to a continuously driven resonator, where the stabilization rate is limited to the resonator decay rate Γ_r and therefore may be orders of magnitude lower than the maximum rate achievable using the QCR.

We test the validity of equation (10) by numerically simulating the system as for figure 3 and fitting an exponential decay to the temporally decreasing deviation. To eliminate the effect of the plateau on the fit, only points where $\delta(t)$ has decreased during all previous interaction phases are included in the fit. The effective rate obtained this way is shown as a function of t_{reset} and t_{int} in figure 4 together with the analytical estimate. The agreement between the simulated and analytical rates suggests that the simplified model successfully captures the essential features of the full master equation (8). The simplified model is less accurate in regions where the attempted stabilization steps are the largest and the assumption $\delta, \theta \ll 1$ does not hold.

The oscillatory behavior as function of t_{reset} is explained by the phase shift mentioned above. In the interaction phase, the complex phase of the qubit state, accumulated during the reset phase due to the dispersive shift, determines the initial direction of the oscillatory motion of the resonator state. The initial direction may be aligned towards the target state or away from it, corresponding to the peaks and valleys in figure 4(a), respectively. Regardless of the alignment of this small initial kick, the state tends to stabilize towards $|\alpha_T\rangle$.

3.4. Resonator initialization by stabilization

Recently, different schemes [15, 16, 19] have been investigated to quickly reset a resonator to the vacuum state. While this is more conveniently achieved by coupling a QCR directly to the resonator, we note that our stabilization sequence may be used for the same purpose in a complementary setup where the QCR is connected to the qubit instead of the resonator. To this end, we apply our stabilization protocol with a target amplitude $\alpha_T = 0$. We study how the stabilization protocol performs if the resonator and the qubit are exposed to heat baths of finite temperatures T_r and T_q , respectively. We consider three cases of experimental interest: (i) the temperature of the bath coupled to the qubit equals T_r ; (ii) the qubit bath is cooled by the QCR to $T_q = T_r/2$; (iii) the qubit bath is cooled to a significantly lower temperature that is independent of T_r . The case (i) is met in an experiment where the qubit is initialized using a heat sink to a heat bath at the same temperature as the electromagnetic environment of the resonator. In case (ii), we assume that the electron temperature of the QCR equals that of the resonator environment, and since the QCR can cool to half of its electron temperature [20], we

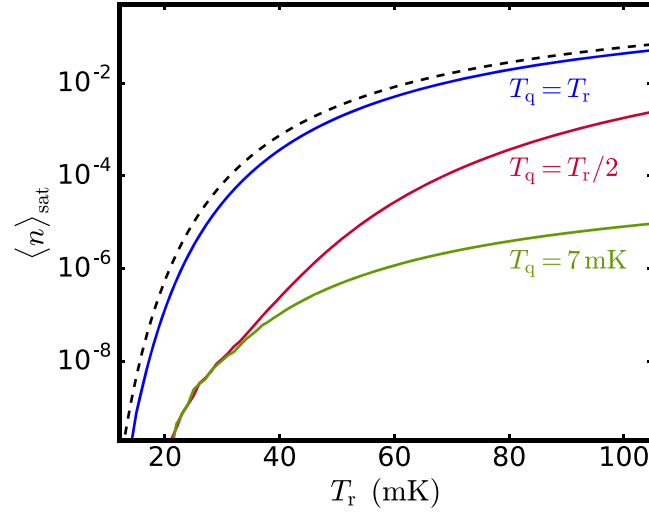


Figure 5. Saturated thermal occupation $\langle n \rangle_{\text{sat}}$ in the stabilized resonator as a function of the resonator bath temperature T_r . The dashed line shows the average number of photons in the initial thermal state, to which 15 iterations of the stabilization sequence are applied to reach $\langle n \rangle_{\text{sat}}$ (solid lines). The temperature T_q of the bath that is coupled to the qubit is studied in the three cases presented in the text, as indicated. The parameters used in the simulation equal those in figure 3.

obtain $T_q = T_r/2$. In case (iii), we assume that the QCR or the heat sink is well thermalized with a very low temperature environment such as the phonon bath of the cryostat (see, e.g., [23]), which may be achieved since the QCR electrons may be shielded from any rf excitation.

We simulate the system by adding the Lindblad terms $\Gamma_q^\dagger(t) \mathcal{L}[\hat{I} \otimes \hat{\sigma}_+] \hat{\rho}(t)$ and $\Gamma_r^\dagger \mathcal{L}[\hat{a}^\dagger \otimes \hat{I}] \hat{\rho}(t)$ to the master equation (8). Here, the excitation rates are given by the detailed balance conditions $\Gamma_q^\dagger(t) = \Gamma_q(t) \exp\left[-\frac{\hbar\omega_q(t)}{k_B T_q}\right]$ and $\Gamma_r^\dagger = \Gamma_r \exp\left[-\frac{\hbar\omega}{k_B T_r}\right]$, where k_B is the Boltzmann constant. We assess the performance of the stabilization sequence on an initial thermal state with a mean thermal occupation of $\langle n(0) \rangle = 1/(\Gamma_r/\Gamma_r^\dagger - 1)$ by evaluating the remaining amount of photons in the resonator after M cycles of stabilization, $\langle n(M) \rangle = \text{Tr}[(\hat{a}^\dagger \hat{a} \otimes \hat{I}) \hat{\rho}(Mt_{\text{cycle}})]$. We find that after 5 or more iterations of the sequence, the thermal occupation saturates to a level shown in figure 5 for each case.

The results suggest that the stabilization sequence can be utilized to decrease the thermal occupation of the resonator several orders of magnitude below the initial equilibrium value, provided that the environment that is coupled to the qubit is colder than the resonator, as in cases (ii) and (iii). Hence, our protocol also works for thermal states, a result that is not evident from the simplified model of coherent states. In case (i), the modest cooling of the resonator is explained by the periodic detuning of the qubit. Changing the qubit frequency abruptly by $+\Delta$ or $-\Delta$ changes the effective temperature of the qubit to be higher or lower compared to the unchanged frequency, respectively, which leads to cooling of the resonator after each interaction phase.

4. Discussion

The results presented above suggest that our method is able to stabilize a coherent or the vacuum state significantly faster than a simple continuous drive. Coupling the resonator to the qubit, and hence indirectly to the tunable electromagnetic environment, allows effective removal of entropy from the resonator mode without directly exposing it to a cold bath. The method is therefore suitable for accelerating state control in cavities or other resonators that are designed for relatively long storage times. As a special case, the method can also be used to reduce the amount of thermal photons in a resonator and thus could be utilized in a resonator initialization protocol in systems where more direct approaches are elusive.

Previously we designed a protocol which also steers the resonator state towards a specific coherent state by employing a series of resonant rotation gates between the resonator and ancillary qubits. In [21], the photon number difference between the target and concurrent resonator states leads to slightly modified rotations and ultimately to a convergence towards the target state. However, the deviation from the target state decreases only polynomially with increasing number of iterations M and individual iterations become less effective for an increasing target photon number. The stabilization sequence presented in this work features three improvements over the previous method: the state convergences exponentially with M , the stabilization rate is ideally independent of the target amplitude, and the sequence can be realized experimentally using readily available devices. Ultimately, the main motivation for the state stabilization in [21] is to reduce the amount of

energy needed in the implementation of quantum gates by repairing the photon state instead of regenerating it for each operation. The current method carries out the same task and scales well in terms of required iterations, but is not optimized to reduce energy consumption. Such study is left for future research.

The stabilization protocol and its approximate model presented here are verifiable using currently available experimental techniques. The temporal decrease of $\delta(t)$ can be assessed by means of a full state reconstruction or by measuring the first moment $\langle \hat{a} \rangle$, which can be routinely carried out [6] with a precision of at least 10^{-3} . As discussed in section 3.2, possible crosstalk can be reduced to a tolerable level for the stabilization protocol. In addition to testing the proposed method experimentally, we will investigate ways to extend the theoretical framework for creation of cat states.

Acknowledgments

We thank A Mäkinen for useful discussions. This work was carried out as part of the Academy of Finland Centre of Excellence program (project 312300). The work was supported by the European Research Council under under Consolidator Grant No. 681311 (QUESS). We also acknowledge funding from the Finnish Cultural Foundation.

Appendix A. Solution of the pendulum equation

In this appendix, we present the closed-form solutions of equations (6) and (7) that are used to derive the analytical result of appendix B. For initial conditions $\theta(0) = \theta_0$ and $\dot{\theta}(0) = 2g|\delta(0)| = 2g|\delta_0|$, the solutions are expressed as

$$\delta(t) = k \operatorname{dn}(gt|k| + \tau, |k|^{-2}), \quad (\text{A1})$$

$$\theta(t) = 2\operatorname{am}(gt|k| + \tau, |k|^{-2}), \quad (\text{A2})$$

where $\operatorname{dn}(x, k)$ and $\operatorname{am}(x, k)$ are Jacobi elliptic functions [24] and

$$k = \delta_0 \sqrt{1 + |\delta_0|^{-2} \sin^2(\theta_0/2)}, \quad (\text{A3})$$

$$\tau = F(\theta_0/2, |k|^{-2}), \quad (\text{A4})$$

with $F(x, k)$ being the incomplete elliptic integral of the first kind [24].

Appendix B. Analytical approximation for the stabilization rate

In this appendix, we provide the derivation of equation (10) for the analytical approximation of the effective stabilization rate. In the following, we define the deviation after the n th interaction phase to be $\delta_n = \delta(t_n)$, and the corresponding qubit-related variable as $s_n = e^{i\phi(t_n)} \sin \frac{\theta(t_n)}{2}$, with $t_n = nt_{\text{cycle}} - t_{\text{reset}}$. In the interaction phase, δ_n and $|s_n|$ evolve according to equations (A1) and (A2), which neglect the dissipation in the system. We first expand equations (A1) and (A2) in the limit of small errors assuming $|k| = \sqrt{|\delta_n|^2 + |s_n|^2} \ll 1$. A straightforward Taylor expansion to the first order in k yields the coupled equations

$$\delta_n = \delta_{n-1} \cos(gt_{\text{int}}) - s_{n-1} \sin(gt_{\text{int}}), \quad (\text{B1})$$

$$s_n = \delta_{n-1} \sin(gt_{\text{int}}) + s_{n-1} \cos(gt_{\text{int}}). \quad (\text{B2})$$

We observe that the effect of the interaction phase is to rotate the vector $v_n = (\delta_n, s_n)^T$ by an angle gt_{int} .

In the reset phase, the probability amplitude s_n of the excited qubit state decays with the increased rate $\Gamma_{q,\text{max}}/2$ and gains a phase shift $\phi(t_n) - \phi(t_{n-1}) = \left(\Delta + \frac{g^2}{\Delta}\right)t_{\text{reset}}$ due to the dispersion. Accounting for the additional dispersive shift $-\frac{g^2}{\Delta}t_{\text{reset}}$ gained by the mode, the system state after n cycles is therefore expressed as

$$v_n = Uv_{n-1} = U^n v_0, \quad (\text{B3})$$

where

$$U = e^{-i\frac{g^2}{\Delta}t_{\text{reset}}} \begin{pmatrix} 1 & 0 \\ 0 & e^{-\kappa t_{\text{reset}}} \end{pmatrix} \begin{pmatrix} \cos(gt_{\text{int}}) & \sin(gt_{\text{int}}) \\ -\sin(gt_{\text{int}}) & \cos(gt_{\text{int}}) \end{pmatrix}, \quad (\text{B4})$$

is the action of a single stabilization cycle. Here, $\kappa = \frac{1}{2}\Gamma_{q,\text{max}} - i\Delta - 2i\frac{g^2}{\Delta}$.

To access Γ_{eff} , we calculate δ_n from v_n with the initial condition $v_0 = \begin{pmatrix} \delta_0 \\ 0 \end{pmatrix}$.

The eigenvalues of U are given by

$$\lambda_{\pm} = e^{-\left(\frac{\kappa}{2} + i\frac{g^2}{\Delta}\right)t_{\text{reset}}}(\mu \pm \sqrt{\mu^2 - 1}), \quad (\text{B5})$$

where

$$\mu = \cosh\left(\frac{1}{2}\kappa t_{\text{reset}}\right) \cos(gt_{\text{int}}), \quad (\text{B6})$$

and the corresponding unnormalized eigenvectors are

$$v_{\pm} = \begin{pmatrix} \cos(gt_{\text{int}}) - \lambda_{\pm} e^{\left(\kappa + i\frac{g^2}{\Delta}\right)t_{\text{reset}}} \\ \sin(gt_{\text{int}}) \end{pmatrix}. \quad (\text{B7})$$

We decompose the initial vector as $v_0 = \frac{\delta_0}{|v_+ - v_-|}(v_+ - v_-)$ and insert it into equation (B3). This yields

$$\begin{aligned} \delta_n &= (1 \ 0) U^n \begin{pmatrix} \delta_0 \\ 0 \end{pmatrix} = \frac{\delta_0}{|v_+ - v_-|^2} \\ &\times [\lambda_+^n (|v_+|^2 - v_-^\dagger v_+) + \lambda_-^n (|v_-|^2 - v_+^\dagger v_-)]. \end{aligned} \quad (\text{B8})$$

In agreement with equation (9), we define the effective stabilization rate after n cycles of stabilization as

$$\Gamma_{\text{eff}}(n) = \frac{-1}{nt_{\text{cycle}}} \ln \left| \frac{\delta_n}{\delta_0} \right|. \quad (\text{B9})$$

We insert equation (B8) into equation (B9). In the limit $n \rightarrow \infty$, the only non-vanishing factor is $\frac{-1}{nt_{\text{cycle}}} \ln |\lambda_{\pm}|$ for $\text{Re}(\mu) \gtrless 0$. Thus

$$\Gamma_{\text{eff}} \approx -\frac{1}{t_{\text{cycle}}} \ln |\lambda_{\pm}| \quad (\text{B10})$$

$$= \frac{\Gamma_{\text{q,max}}}{4} \frac{t_{\text{reset}}}{t_{\text{cycle}}} - \frac{1}{t_{\text{cycle}}} \ln |\mu \pm \sqrt{\mu^2 - 1}| \quad (\text{B11})$$

which is the result claimed in equation (10).

References

- [1] Kimble H J 2008 *Nature* **453** 1023
- [2] Hofheinz M *et al* 2009 *Nature* **459** 546
- [3] Mariantoni M *et al* 2011 *Nat. Phys.* **7** 287
- [4] Blais A, Huang R-S, Wallraff A, Girvin S M and Schoelkopf R J 2004 *Phys. Rev. A* **69** 062320
- [5] Wallraff A, Schuster D I, Blais A, Frunzio L, Majer J, Devoret M H, Girvin S M and Schoelkopf R J 2005 *Phys. Rev. Lett.* **95** 060501
- [6] Eichler C, Bozyigit D, Lang C, Steffen L, Fink J and Wallraff A 2011 *Phys. Rev. Lett.* **106** 220503
- [7] Lund A P, Ralph T C and Haselgrove H L 2008 *Phys. Rev. Lett.* **100** 030503
- [8] Vlastakis B, Kirchmair G, Leghtas Z, Nigg S E, Frunzio L, Girvin S M, Mirrahimi M, Devoret M H and Schoelkopf R J 2013 *Science* **342** 607
- [9] Leghtas Z, Kirchmair G, Vlastakis B, Schoelkopf R J, Devoret M H and Mirrahimi M 2013 *Phys. Rev. Lett.* **111** 120501
- [10] Yin Y *et al* 2013 *Phys. Rev. Lett.* **110** 107001
- [11] Pierre M, Svensson I-M, Sathyamoorthy S R, Johansson G and Delsing P 2014 *Appl. Phys. Lett.* **104** 232604
- [12] Sirois A J, Castellanos-Beltran M A, DeFeo M P, Ranzani L, Lecocq F, Simmonds R W, Teufel J D and Aumentado J 2015 *Appl. Phys. Lett.* **106** 172603
- [13] Pfaff W, Axline C J, Burkhardt L D, Vool U, Reinhold P, Frunzio L, Jiang L, Devoret M H and Schoelkopf R J 2017 *Nat. Phys.* **13** 882
- [14] Flurin E, Roch N, Pillet J D, Mallet F and Huard B 2015 *Phys. Rev. Lett.* **114** 090503
- [15] Bultink C C *et al* 2016 *Phys. Rev. Appl.* **6** 034008
- [16] McClure D T, Paik H, Bishop L S, Steffen M, Chow J M and Gambetta J M 2016 *Phys. Rev. Appl.* **5** 011001
- [17] Sarlette A, Raimond J M, Brune M and Rouchon P 2011 *Phys. Rev. Lett.* **107** 010402
- [18] Leghtas Z *et al* 2015 *Science* **347** 853
- [19] Tan K Y, Partanen M, Lake R E, Govenius J, Masuda S and Möttönen M 2017 *Nat. Commun.* **8** 15189
- [20] Silveri M, Grabert H, Masuda S, Tan K Y and Möttönen M 2017 *Phys. Rev. B* **96** 094524
- [21] Ikonen J, Salmilehto J and Möttönen M 2017 *npj Quantum Inf.* **3** 17
- [22] Johansson J, Nation P and Nori F 2013 *Comput. Phys. Commun.* **184** 1234
- [23] Feshchenko A V, Casparis L, Khaymovich I M, Maradan D, Saira O-P, Palma M, Meschke M, Pekola J P and Zumbühl D M 2015 *Phys. Rev. Appl.* **4** 034001
- [24] Abramowitz M and Stegun I 1972 *Handbook of Mathematical Functions and Formulas, Graphs, and Mathematical tables* 9th edn (New York: Dover)